Cold Regions Science and Technology, 6 (1983) 195–206
Elsevier Scientific Publishing Company, Amsterdam – Printed in The Netherlands

ESTIMATION OF COMBINED ICE AND WIND LOAD ON OVERHEAD TRANSMISSION LINES

Pierre McComber, Gilles Morin
Université du Québec à Chicoutimi, Chicoutimi, Québec, G7H 2B1 (Canada)
Richard Martin and Luong Vo Van
Hydro-Québec, Montréal, Québec (Canada)

(Received March 10, 1982; accepted in revised form August 3, 1982)

ABSTRACT

In recent years, the design of high-voltage transmission lines has been increasingly optimized. In areas where ice accretion on conductors is possible, the load resulting from added weight or increased aerodynamic forces becomes an important design parameter. At present, calculations for combined ice–wind loads do not take the effect of accretion shape into account. In this study, ice accretions are formed on a conductor in a wind tunnel for three types of ice: soft rime, hard rime and glaze. Aerodynamic vertical and horizontal forces are then measured for different wind velocities. It is shown that when the wind remains in the direction of ice build-up, the aerodynamic force due to the asymmetric shape is responsible for a significant increase in the total force and that the present combined ice–wind load calculations can dangerously underestimate the risk of an overload.

1. INTRODUCTION

High-voltage transmission lines are subjected, like all structures, to wind-loading. Adequate meteorological data is available to evaluate this design factor in most regions. However, in certain climatic areas, there is an added hazard of rime and glaze accretions on transmission lines (Bourgsdorf et al., 1968). In these areas, glaze and rime has to be taken into account in the design (Ghannoum, 1981) even though at the moment little or no statistical meteorological data is available on ice accretions in areas where the transmission lines are set up. Moreover, ice and wind have a combined effect resulting in increased wind-loading. In these cases not only the weight but also the shape of the ice accretion has an important effect on the total load (Bassarskaya et al., 1981).

Most of the research that has been conducted on the combined effect of ice and wind has been related to wind-induced vibrations (Blevins, 1977). Wind-induced vibrations of the type referred to as galloping require an asymmetric shape which is obtained only when conductors are covered with an ice accretion. Since these vibrations start even for a thin layer of ice, these studies have not considered heavy loading due to ice.

For the calculations of the combined static load, the shape of the accretion is important, and there is practically no study existing to determine possible ice accretion shape of a type large enough to create an overload.

In this paper, the design criteria used by a hydroelectric power company (Hydro-Québec) to predict wind and ice combined loading are compared with loads measured for wind tunnel accretions.

2. PRESENT METHOD FOR THE CALCULATION OF WIND AND ICE LOADS

Recent Hydro-Québec transmission lines are designed to withstand some limit loads. The first one, a wind load on bare cables, consists of a wind speed of 136.8 km/h (85 mph). A second load consists of a maximum radial ice thickness of 4.45 cm

0165-232X/83/$03.00

(1.75 in.) with no wind. Another load consists of combined wind and ice: 3.18 cm (1.25 in.) of ice with a wind speed of 72.4 km/h (45 mph). These loads are all assumed to have a return period of at least 50 years. For these conditions the forces are calculated as follows.

Wind limit force

The limit horizontal or drag force due to the wind on a bare conductor is calculated by the following relation:

$$F_h = 0.6469\, D_0 V^2 \quad (1)$$

where F_h is the horizontal force (N/m); D_0 the conductor diameter (m); V the wind velocity (m/s).

Ice limit force

The ice on a conductor adds weight. An increased vertical force (N/m), F_v, is calculated by adding the weight of ice W_i to the weight of the conductor W_c:

$$F_v = W_c + W_i \quad (2)$$

Combined limit force

The calculation of the combined limit load is based on the assumption of a cylindrical shape for the ice accretion. This shape has no positive or negative aerodynamic lift forces so that the vertical force is simply calculated by eqn. (2). The horizontal force is obtained from eqn. (1) using a modified diameter to account for the ice. The volume and weight of the ice are related by the following expression:

$$\frac{\pi}{4}(D^2 - D_0^2) = \frac{W_i}{\rho_i g} \quad (3)$$

in which ρ_i is the ice density (0.92).

The horizontal and vertical forces are then added vectorially to yield the total force:

$$F_T = (F_h^2 + F_v^2)^{1/2} \quad (4)$$

3. AVAILABLE DATA ON WIND AND ICING LOADS

In order to be able to evaluate combined wind and ice loads, statistical meteorological data on ice thicknesses as well as wind speeds during icing or immediately after must be considered. Unfortunately, there is no reliable data at the present on ice accretion thicknesses. Measurements of ice accretion thicknesses have recently started to be taken. Wind speeds have been measured for a much longer time. Table 1, for example, shows the annual maximum wind speeds obtained during icing precipitations and the period during which the temperature is below 0°C with a maximum of 72 hours, for a few Canadian airports.

TABLE 1

Maximum annual wind speed (km/h) as a function of the recurrence interval (years)

	Recurrence interval (years)						
	2	5	10	25	50	100	150
Bagotville (24 years)	14.8	17.0	18.3	20.1	21.5	22.8	23.7
Dorval (24 years)	14.3	17.0	18.8	21.0	22.8	24.6	25.0
Goose (24 years)	13.9	16.1	17.9	20.1	21.5	23.3	23.7
Knoblake (24 years)	15.2	17.9	20.1	22.8	24.6	26.8	27.3
Mont-Joli (24 years)	15.7	18.8	20.6	22.8	24.6	26.8	27.3
Ottawa (23 years)	13.4	16.1	17.9	20.1	21.5	23.3	23.7
Sept-Iles (24 years)	17.4	20.6	22.4	24.1	26.4	28.2	29.1
Val d'Or (24 years)	10.7	12.5	13.9	15.2	16.1	17.4	17.9

4. COMPARISON OF WIND TUNNEL AND FIELD SAMPLES

Ice accretion samples were obtained in a refrigerated wind tunnel having a test section of 0.61 × 0.61 m. Samples were formed on a conductor (3.5 cm in diameter) with 20 strands on the outside layer, and a weight of 21.46 N/m (Hydro-Québec BERSMIS conductor).

Supercooled droplets

Six nozzles were used in the wind tunnel to produce the supercooled droplets 3 m upstream of the test section before the contraction (air atomizing

nozzles #30, fluid cap #40100, air cap #120-6-35-60). The air and water pressures were adjusted in the nozzles to give the good combination of water content and droplet diameter required to produce either rime or glaze. A spectrum of droplet diameters was obtained for each nozzle setting using the silver colloid film method (Godard, 1960). For example, a mean volume diameter of 24.3 μm was used to produce soft rime.

Water content

The water content of the air was measured by the single-cylinder method (Rush and Wardlaw, 1957). From the weight of ice accumulated on a 3.15 mm radius cylinder during a short period of time (30 s to 1 min), the water content is evaluated by the following equation:

$$m = \frac{\pi}{\nu_i EVT}\left[\left(\frac{\nu_i w}{\pi l} + r_i^2\right)^{1/2} - r_i\right] \qquad (5)$$

where m is the water content (g/m^3); T the accumulation time (s); V the air speed (m/s); ν_i the specific volume of the rime (cm^3/g); w the mass of accumulated ice (g); r_i, l and E are the radius (cm), length (cm) and collection efficiency of the cylinder respectively.

Ice accretion samples

For the wind tunnel ice accretion experiments, the conductor was supported at each end by ball bearings and a small metal rod was used as a torsion spring to control the rotation of the conductor during ice formation. A 1.9 mm steel rod, 21.4 cm long, was used as a spring. This simulates the torsional rigidity existing in the center of a 70 m sub-span. A sub-span is defined as the length of conductor between spacer-dampers on a four-conductor bundle.

Comparison of different ice accretion shapes

Figure 1 shows an ice accretion obtained on a fixed cylinder in the wind tunnel. In Fig. 2 a two-conductor bundle is shown (Kellow and Martin, 1976); it remained almost fixed during ice formation, the torsional rigidity being much greater. It is clear from the photograph that whenever the

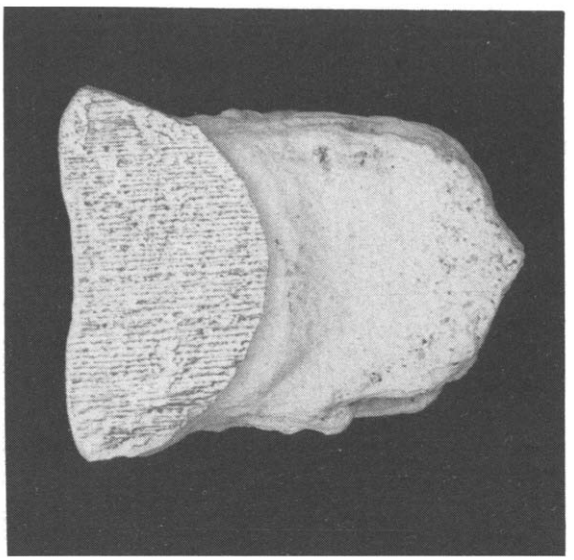

Fig. 1. Ice accretion obtained on a fixed cylinder in a wind tunnel, showing the accretion on the right and half of the cylinder on the left.

conductor is not permitted to rotate and the wind is steady in its direction, the ice forms on one side only of the conductor. This is explained by the fact that supercooled droplets hit the iced surface only on the front part of an exposed object (McComber and Touzot, 1981).

Long conductors, however, can usually rotate somewhat around their axis under the weight of the ice formed. This can be verified on natural ice samples. Figure 3 is a photograph under polarized light of an accretion cross-section. This sample was collected by Hydro-Québec in the Baie-Comeau area after glaze was formed on transmission lines, April 6th, 1981. For a fixed cable, ice crystals would grow almost radially; the spiraled growth visible in Fig. 3 is a result of a torsion of the cable while the ice was building up. Figure 4 shows samples that were obtained in the wind tunnel with the torsion spring described above. Figure 5 shows shapes of ice accretion obtained on a six-conductor bundle, also in a wind tunnel, with an experimental set-up permitting a small rotation of the bundle under the weight of ice. Figure 6 is a photograph of a field sample collected by Hydro-Québec. On this occasion, a four-conductor bundle (spacing between conductors: 457 mm) twisted on itself.

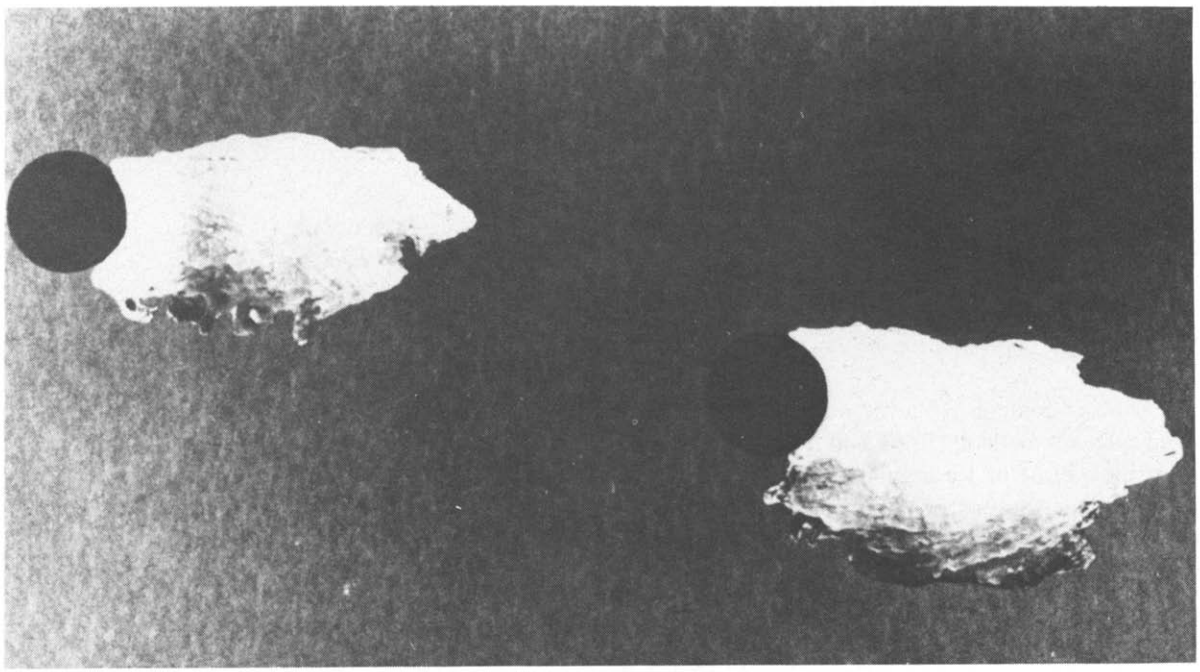

Fig. 2. Photograph of the cross-section of ice accretion on a two-conductor bundle after 15.75 h of icing in a wind tunnel.

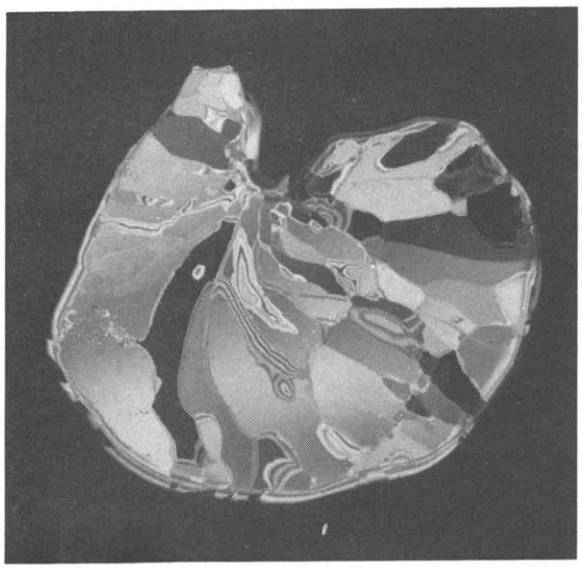

Fig. 3. Photograph under polarized light of a transmission line accretion formed in the Baie-Comeau area (6/4/81).

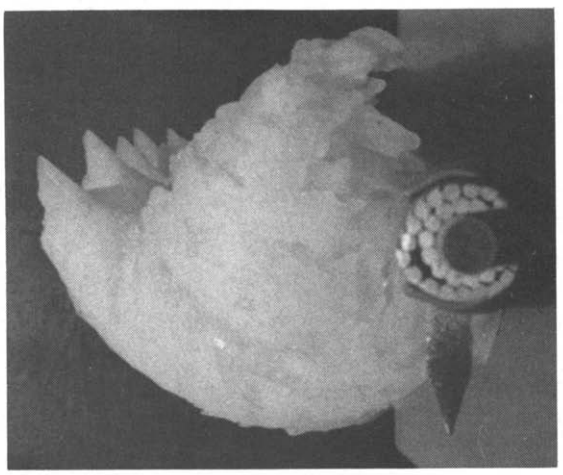

Fig. 4. Photograph of ice accretion obtained on a cylinder permitted to rotate in a wind tunnel.

Even if one considers the possibility of slight changes in the wind direction, such a shape is again best explained by the torsion of the conductor thus permitting ice build-up on approximately 180° around the conductor.

5. INSTRUMENTATION AND CALIBRATION

Temperature and wind speed measurements

Temperatures are measured in the wind tunnel

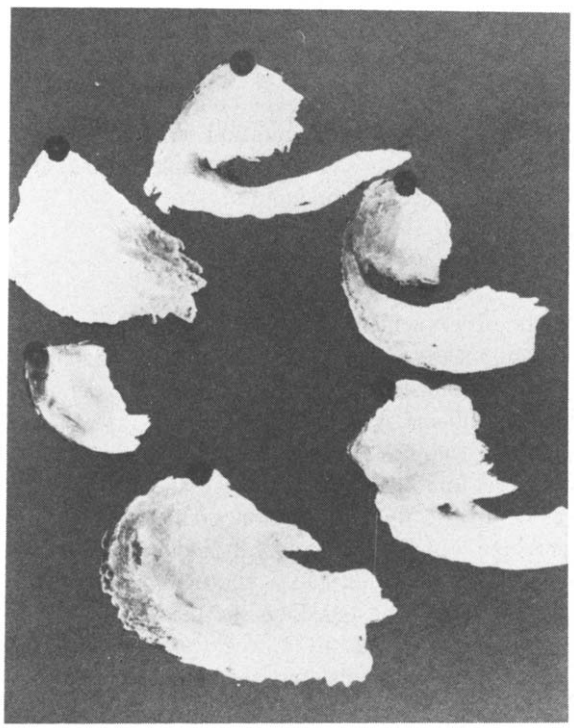

Fig. 5. Photograph of cross-section of ice accretion of a six-conductor mini-bundle after 20.25 h of icing in a wind tunnel.

with a thermometer (± 0.5°C). Wind speeds are measured with a Pitot tube (Dwyer no. 160, 7.9 mm diameter). The accuracy of the water manometer was 0.64 mm, giving an approximate maximum error of 15% for the lowest velocities measured.

Lift force and drag force measurements

Vertical forces on ice-covered conductors are measured with a load cell Interface Inc. B50, while the drag force is measured by strain gauges (Intertechnology, EA-13-125AD-12C E) mounted on thin plates of metal. The set-up permits the uncoupling of the drag and lift forces by blocking the vertical deflection while the horizontal force is measured and vice versa.

A resistance bridge and an amplifier (10 channel) are used to handle the signal (Intertechnology Ltd., Vishay no. 2100). The signals are then recorded on a graph by a pen recorder.

End effects for the measurements of drag and lift forces on a short cylinder

Since the drag and lift forces are measured in a

Fig. 6. Photograph of the ice accretion formed on an actual transmission line conductor (25/2/78) in the Québec City area.

wind tunnel, one must consider end-effect corrections, the experimental length being relatively short. This correction accounts for the wind speed and the shape of an object. For a cylinder and a wind speed equivalent to $Re = 8.8 \times 10^4$, Goldstein (1965) gives a correction factor reproduced on Fig. 7. This correction factor was used to modify the wind tunnel measurements in order to obtain the results applicable for a large L/D ratio.

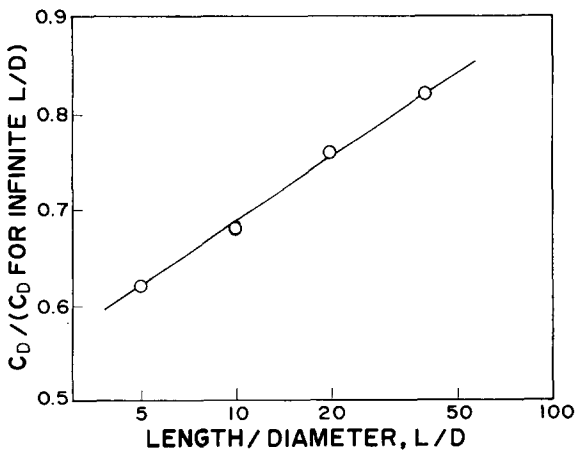

Fig. 7. Correction factor on the drag coefficient for finite length cylinder (Goldstein, 1965).

Force measurements verification

A calibration check was made by measuring the drag coefficient of a 3.49 cm diameter cylinder. Figure 8 compares the drag coefficient obtained with the wind tunnel set-up and results obtained by various authors and reported by Goldstein (1965). The experimental values of the drag force were first corrected for end effects. The comparison on Fig. 8 indicates that the instrumentation set-up to measure forces was adequate and could be applied to measurements on ice-covered conductors.

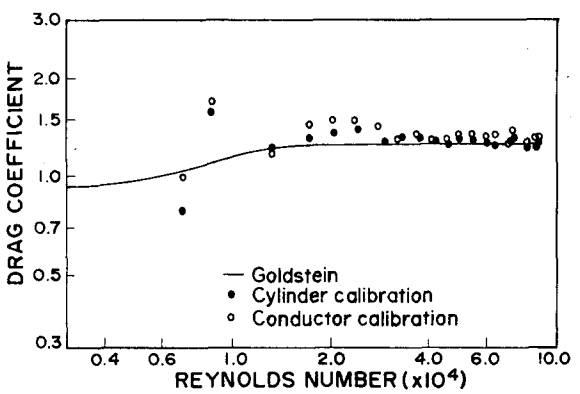

Fig. 8. Cylinder and conductor drag coefficient as a function of Reynolds number.

Experimental procedure

The experiment was done in two steps: ice formation and measurement on the sample using wind only. Once the adjustments were made for temperature, wind speed and water content of the flow, the ice accretion samples were formed using the torsion spring set-up. The size of the ice accretion sample was controlled by the duration of the icing period. Once the sample was formed, its dimensions and weight were recorded and a photograph was taken.

It was then reinstalled on the measurement support, and drag and lift forces were measured at different wind speeds for the different samples. The measurements were made for speeds up to 37 m/s or until the ice accretion shattered under the effect of high wind speeds.

6. RESULTS

In order to obtain information on the behavior of different types of ice, conductors were covered in succession by soft rime, hard rime and glaze. Also, in order to verify how these results could be reproduced in the wind tunnel, the soft rime experiments were done three times for each thickness. Finally, for each type of ice, experiments were done for three sizes. The meteorological parameters for these experiments are summarized in Table 2. These conditions were chosen in order to simulate as closely as possible the natural conditions of icing. However, tests being made in a wind tunnel, certain conditions had to be adjusted to correspond to realistic parameters in the wind tunnel. The accretion had to take place somewhat faster, which is made possible by using a higher water content and a lower temperature. As far as glaze is concerned it had to be made at a velocity higher than that which is usually encountered in nature. The shape of glaze accretion is therefore less realistic than the rime accretion.

Figures 9, 10 and 11 show the drag and lift forces as a function of velocity for the three sizes of soft rime. The three curves appearing on each figure correspond to the three samples made for each size. Figures 12 and 13 show the same type of results for hard rime and glaze respectively.

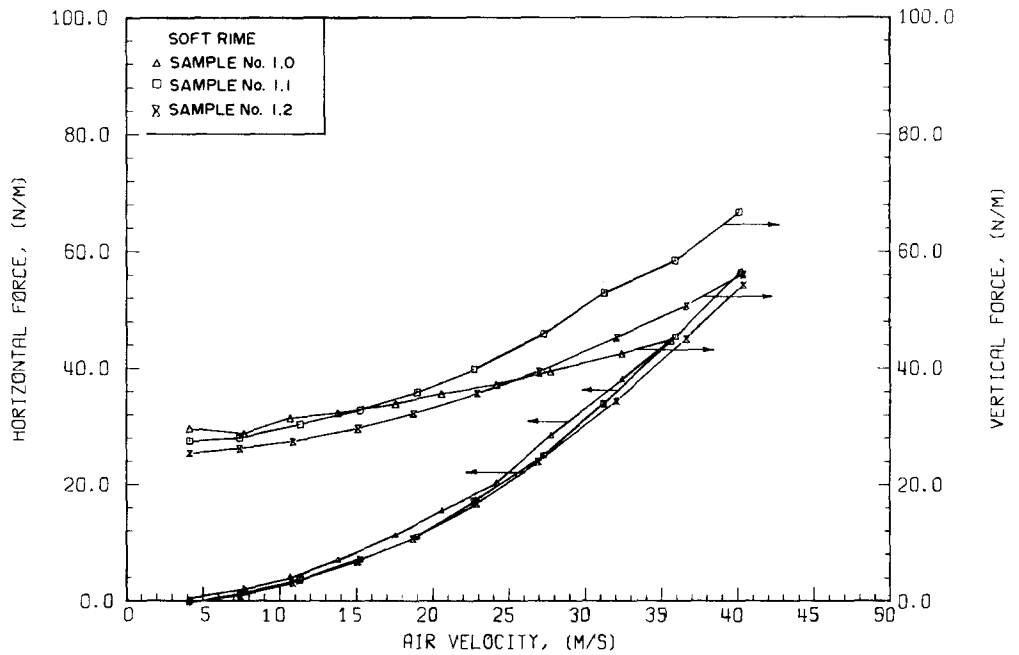

Fig. 9. Horizontal and vertical forces on soft rime accretion ($D \cong 45$ mm) as a function of air velocity.

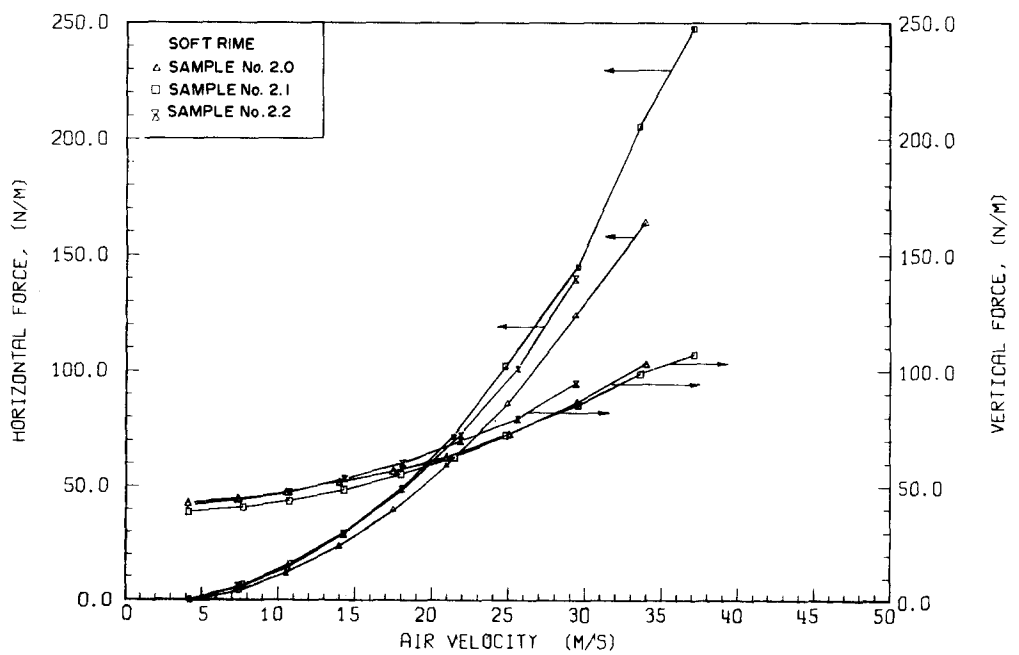

Fig. 10. Horizontal and vertical forces on soft rime accretion ($D \cong 65$ mm) as a function of air velocity.

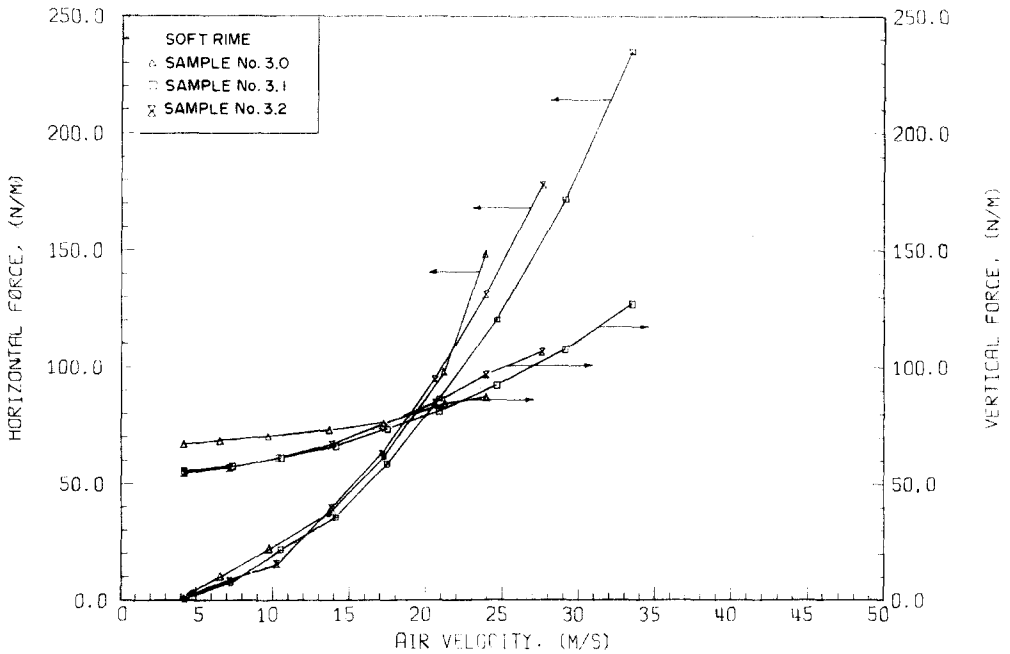

Fig. 11. Horizontal and vertical forces on soft rime accretion ($D \cong 80$ mm) as a function of air velocity.

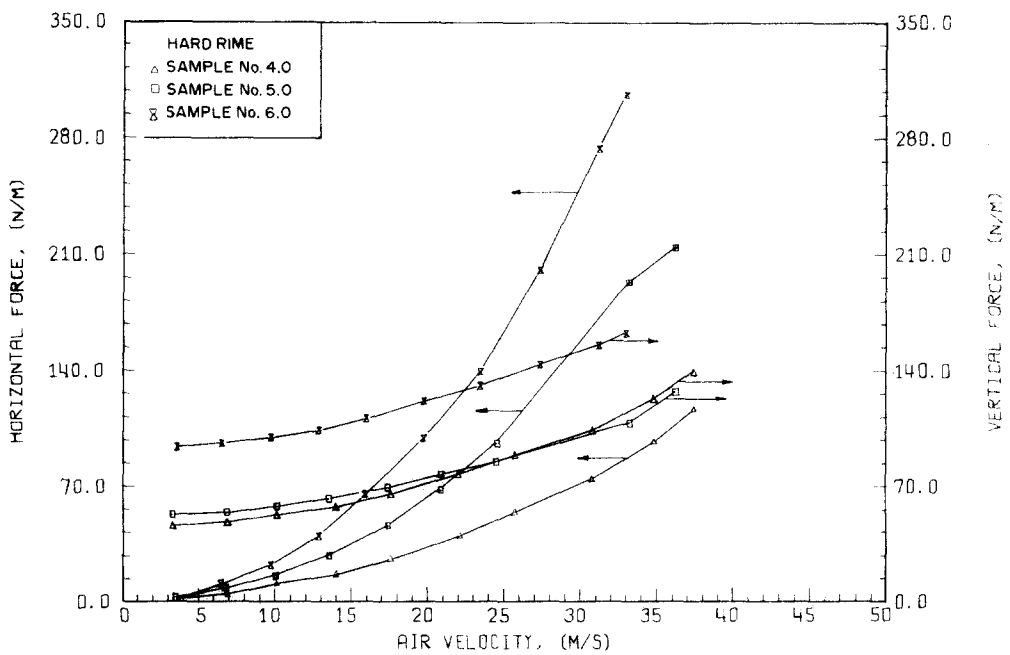

Fig. 12. Horizontal and vertical forces on hard rime accretion as a function of air velocity.

7. COMPARISON OF CALCULATED AND EXPERIMENTAL WIND AND ICE LOAD

In Table 3 a comparison is made of the calculated drag and lift forces from eqns. (1) and (2) with the wind tunnel measurements. This comparison is made for two wind speeds: 22.35 m/s (50 mph) and 26.82 m/s (60 mph) and for the medium size accretion

TABLE 2

Wind tunnel conditions during conductor icing

	Type of ice														
	Soft rime									Hard rime			Glaze		
Sample number	1.0	1.1	1.2	2.0	2.1	2.2	3.0	3.1	3.2	4	5	6	7	8	9
Temperature (°C)	−15.0	−15.5	−15.5	−15.0	−15.0	−15.0	−15.0	−15.5	−15.5	−11.0	−11.0	−11.0	−6.0	−6.0	−6.0
Liquid water content (g/m^3)	2.9	2.9	2.9	2.9	2.9	2.9	2.9	2.9	2.9	2.5	2.5	2.5	1.9	1.9	1.9
Wind speed (m/s)	5.58	5.63	5.63	5.58	5.63	5.63	5.58	5.63	5.63	7.75	7.75	7.75	12.55	12.55	12.55
Duration of accretion (h:min)	1:00	1:00	1:00	2:15	2:15	2:15	4:00	3:50	3:50	1:30	2:30	4:30	1:00	1:35	2:45
Rotation angle (deg.)	20	18	18	87	85	85	117	114	114	55	100	153	30	55	110
Accretion weight (N/m)	7.66	6.20	4.38	23.27	19.48	21.59	47.35	35.38	34.36	23.71	30.57	71.86	25.97	44.28	95.93
Calculated equivalent diameter* (mm)	48.0	45.7	42.9	67.1	63.0	65.3	88.9	78.8	77.9	67.6	74.4	106.6	69.9	86.5	121.5

*In all cases the equivalent diameter was calculated assuming a 0.9 specific weight for ice, using a 35 mm conductor.

TABLE 3

Comparison of calculated and experimental ice–wind loads

Forces	Wind speed (m/s)																
	22.35 m/s (50 mph)									26.37 m/s (59 mph)							
	Calculated forces eqns. (1), (2), (4)			Measured forces			Ratio			Calculated forces eqns. (1), (2), (4)			Measured forces			Ratio		
	F_h	F_v	F_T	F'_h	F'_v	F'_T	F'_h/F_h	F'_v/F_v	F'_T/F_T	F_h	F_v	F_T	F'_h	F'_v	F'_T	F'_h/F_h	F'_v/F_v	F'_T/F_T
Sample #2 (soft rime)	20.1	45.4	49.7	67.2	65.6	93.9	2.99	1.44	1.89	28.0	45.4	53.3	98.4	76.8	124.8	3.51	1.69	2.34
Sample #4 (hard rime)	20.3	45.8	50.1	39.6	84.6	92.9	1.95	1.83	1.85	28.2	45.8	53.8	58.3	95.6	112.0	2.06	2.09	2.08
Sample #8 (glaze)	26.0	65.7	70.7	54.3	67.1	86.3	2.09	1.02	1.22	36.1	65.7	75.0	77.0	68.5	103.1	2.13	1.04	1.37

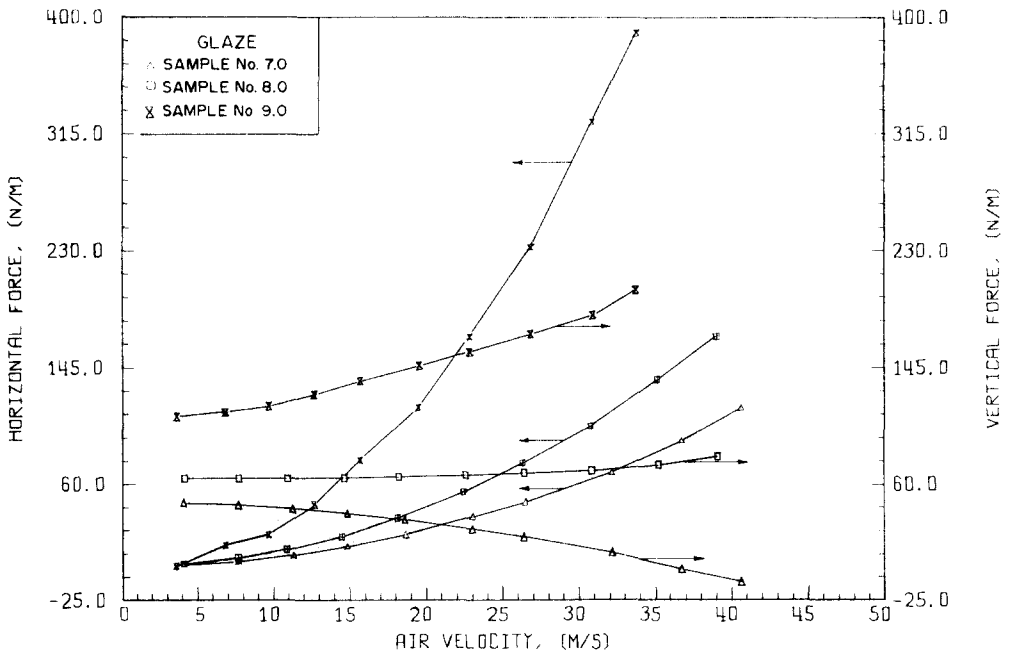

Fig. 13 Horizontal and vertical forces on glaze accretion as a function of velocity.

(~ 20 mm radial ice) of soft rime, hard rime and glaze. The resulting ratio of experimental to calculated forces is also shown.

From the results of Table 3, a comparison of the loads is made in Fig. 14 for a four-conductor bundle (conductors diameter 35 mm) with a span of 488.8 m (1600 ft). This example is calculated for hard rime (sample #4) with a wind speed of 22.35 m/s (50 mph). Typically, for the suspension assembly, a loading of 38 mm (1.5 in.) radial ice calculated with no wind results in a load of 163 kN. Such an ice thickness has a return period of approximately 50 years. Figure 14 indicates that approximately 16.3 mm (0.66 in.) of radial ice thickness results in a 181.6 kN loading, and this thickness is reached for conditions much more frequent (10 to 25 years return period).

Figure 14 also compares as an example the resulting tension force in the dead end assembly. This force is calculated from the total combined force using a catenary equation. The force obtained is 132% of the limit load permitted on the conductor and 86% of its ultimate tensile strength (UTS).

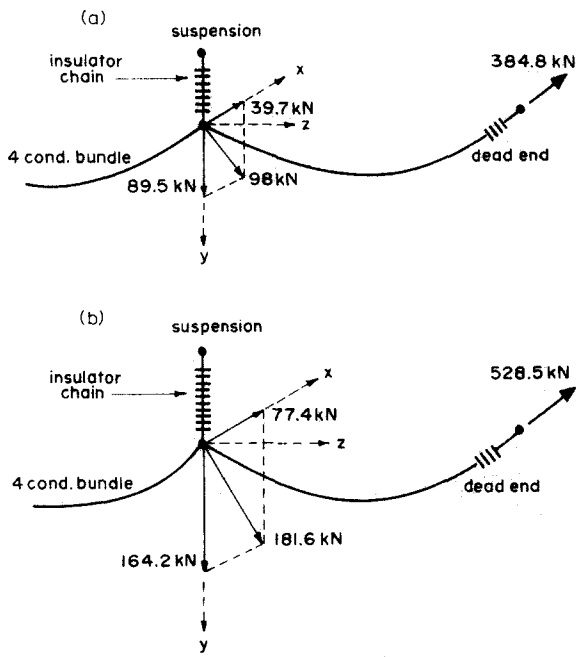

Fig. 14. Example of a comparison of the combined loads for a four-conductor bundle with a 488.8 m span: (a) loads evaluated using eqns. (1) and (2); (b) loads calculated from wind tunnel data for lift and drag forces.

8. DISCUSSION

The comparison in Table 3 indicates that the measured horizontal and vertical forces are larger than the calculated ones in all cases. Since an identical weight is used for the comparison, the difference can be attributed to the aerodynamic forces.

The measured horizontal force is larger for two reasons. First a cross-section of the type shown in Figs. 3–6 offers an increased drag force when compared with the same weight distributed in a cylindrical shape. In all cases these shapes are due to the fact that under the combined effects of weight and torsional rigidity of the cable, ice accumulates mostly under the cylinder, creating a shape which has a larger wind resistance.

The second reason for an underestimation of the calculated horizontal force is that for soft and hard rime the specific weight is lower than 0.9. For the same weight, natural ice accretion will therefore have a larger volume resulting in a larger drag force.

The aerodynamic vertical or lift force is nonexistent for an axisymmetrical shape. The calculated vertical force is obtained only from the ice and conductor weights. The asymmetrical shape, however, creates a lift force. In all the tests except one for glaze, the lift force obtained was negative and therefore equivalent to an added weight. The shapes responsible for this negative lift are again the result of ice weight and torsional rigidity of the cable. As far as the exception (sample #7) is concerned it must be pointed out that the shapes obtained for glaze are less realistic than those for soft and hard rime since, for glaze, the wind speed had to be increased in order to prevent icicles from blocking the test section.

The torsional rigidity of the cable is a determinant factor in the shape of the ice accretion. It can be verified that for a fixed conductor and steady wind the accretion forms only on the front part (Fig. 1). On the other hand, if the rigidity constant was zero, the conductor would rotate as soon as an unbalanced weight is created, and the rotation would then rapidly exceed 360° and a spiraled shape, close to a cylindrical shape, would be formed. The rigidity of real cables is between these two extreme cases, and furthermore it varies along the span of a transmission line since the supports will increase the rigidity at certain locations.

The results presented were obtained for one value of the rigidity constant. Since the final shape of an ice accretion depends strongly on the time history of ice build-up, it will remain difficult to predict the aerodynamic forces on a transmission line. The results presented above are an indication of the importance of aerodynamic forces due to the asymmetrical shape of the ice accretions. This importance is such that even if these forces are difficult to predict accurately, they should not be ignored in the calculations of combined ice–wind loads.

9. CONCLUSIONS

Ice accretions are usually not uniformly distributed around conductors of transmission lines. This has been observed on real transmission lines, and verified in wind tunnels. The usual method of combined wind and ice load calculation has two disadvantages. When a symmetrical shape is assumed around the conductor, drag forces are underestimated while lift forces are not considered. These forces are often very important. Secondly, the assumption that the density is 0.9 Mg/m^3 for all types of ice underestimates soft rime thicknesses and this results in underestimated overall loads as well.

In order to be able to make accurate calculations of combined loads for ice-covered conductors a 'shape factor' should be taken into consideration; if this is not done the total load can be dangerously underestimated.

ACKNOWLEDGMENT

The present work was done by the University of Québec in Chicoutimi under a contract from Hydro-Québec.

REFERENCES

Bassarskaya, T.A., Gohkova, T.N., Lomilina, L.F., Nikiforov, E.P. and Toporkova, G.D. (1981), Ice and ice–wind loads on conductors of overhead transmission lines, Int. Conf. on Large High Voltage Electric Systems, Stockholm, S-22-81-111-08, p. 5.

Blevins, R.D. (1977), Flow-Induced Vibrations, Van Nostrand Reinhold, New York, pp. 55–88.

Bourgsdorf, V.V., Nikiforov, E.P. and Zelitchenko, A.S. (1968), Charge de givre sur les lignes aériennes, Int. Conf. on Large High Voltage Electric Systems, Paris, Vol. 2, pp. 1–8.

Ghannoum, E. (1981), A rational approach to a structural design of transmission lines, IEEE, Power Engineering Soc., Winter Meeting, paper 81WM-224-5, p. 15.

Godard, S. (1960), Mesure de gouttelettes de nuage avec un film de collargol, Bull. Observ. du Puy-de-Dôme, 2: 41–46.

Goldstein, S. (Ed.) (1965), Modern Developments in Fluid Dynamics, Dover Publications, New York, pp. 401–440.

Kellow, M. and Martin, R. (1976), Characteristics of the icing of bundle conductors, IEEE PES, Winter Meeting, paper A-76-088-5.

McComber, P. and Touzot, G. (1981), Calculation of the impingement of cloud droplets in a cylinder by the finite element method, J. Atmos. Sci., 38: 1028–1036.

Rush, C.K. and Wardlaw, R.L. (1957), Icing measurements with a single rotating cylinder, National Aeronautical Establishment of Canada, Lab. Rept. No. LR-206, p. 11.